metals

MDPI

Article

A 4340 Steel with Superior Strength and Toughness Achieved by Heterostructure via Intercritical Quenching and Tempering

Yi Sang [1], Guosheng Sun [2,*] and Jizi Liu [2,3,*]

[1] Nanjing Metro Operation Co., Ltd., Nanjing 211135, China; syf_29@126.com
[2] Nano and Heterogeneous Materials Center, School of Materials Science and Engineering, Nanjing University of Science and Technology, Nanjing 210094, China
[3] Materials Analysis and Test Center, Nanjing University of Science and Technology, Nanjing 210094, China
* Correspondence: gssun@njust.edu.cn (G.S.); jzliu@njust.edu.cn (J.L.)

Abstract: The conventional 4340 steel was used after quenching and tempering, strengthened by the classical pearlitic structure where cementite particles are dispersed through the ferrite matrix. In the present study, a heterostructure microstructure consisting of micro-sized residual ferrite zones and pearlitic zones was introduced by an optimized process of intercritical quenching and tempering, resulting in a steel with higher strength and better toughness. The pearlite steel has a tensile strength of 1233 MPa, yield strength of 1156 MPa, and toughness of 121.5 MJ/m^3. Compared with the pearlite steel, the tensile strength and yield strength of the heterostructure steel have been improved by 67 MPa and 74 MPa, respectively, while the toughness has been increased by 52.5 MJ/m^3. In this heterostructure, the micro-sized ferrite bulks serve as the soft zones surrounded by the hard zones of the pearlite structure to achieve a remarkable work-hardening capacity. Statistical analysis shows that the heterostructure has the best hetero-deformation-induced (HDI) hardening capability when the residual ferrite bulk contributes ~31% by volume fraction, and the quenching temperature is around 780 °C. This study opens new ways of thinking about the strengthening and toughening mechanism of heat treatment of medium carbon steels.

Keywords: 4340 steel; heterogenous microstructure; intercritical quenching; HDI hardening; strengthening mechanism

Citation: Sang, Y.; Sun, G.; Liu, J. A 4340 Steel with Superior Strength and Toughness Achieved by Heterostructure via Intercritical Quenching and Tempering. *Metals* **2023**, *13*, 1139. https://doi.org/10.3390/met13061139

Academic Editor: Igor Yu. Litovchenko

Received: 29 May 2023
Revised: 13 June 2023
Accepted: 17 June 2023
Published: 19 June 2023

1. Introduction

As a high-quality quenched and tempered steel, 4340 alloys have been widely used in various industrial applications such as aircraft landing gear, harmonic reducer flexsplines, and transmission shafts, due to its favorable combination of strength and toughness [1–3]. These mechanical components, which are subjected to high pressure and adverse alternating loads, usually operate in harsh environments where superior overall performance is expected. The 4340 low-alloy steels are alloyed with Cr, Ni, Mo, and Mn elements, to provide good hardenability and fatigue resistance [4,5]. The addition of Cr, Ni, and other elements can improve the hardenability of the alloy and improve the strength and toughness of ferrite in the microstructure, while Mo and Cr elements can promote the formation of carbide, inhibit the growth of austenite grains and prevent tempering brittleness.

Before quenching, this steel is usually normalized to completely dissolve all carbon and other alloying elements. Traditionally, austenitizing, by heating the steels to a temperature above the A_{c3} point, is designed to obtain a fully austenitic structure at a high temperature. The austenitized steel is cooled quickly, such as by quenching in water or an oil bath, and the dissolved carbon does not have enough time to diffuse out of the lattice despite lattice transformation, so the carbon element remains forcibly dissolved in the forming ferrite lattice, forming a tetragonally expanded lattice structure called martensite. During the subsequent tempering process, the diffusion and redistribution cause the

quenched martensite to gradually decompose into cementite and/or carbide embedded in the ferrite matrix, resulting in various combinations of strength and toughness. The trade-off between strength and toughness depended on the morphology, size, distribution, and composition of the embedded cementite (or carbide) and was achieved by tuning the tempering temperature and holding time [1,6]. However, a compromise between material properties is becoming an urgent need due to the booming industries, and it is imperative to make a breakthrough in the traditional quenching and tempering treatment process, so as to establish a new strengthening–toughening mechanism.

A strategy of structural heterostructuring is an emerging trend to develop new metallic materials with superior performance that cannot be achieved by manipulating atomic or phase composition in homogeneous counterparts [7–9]. Heterostructured metallic materials consist of heterogeneous zones with dramatic variations in mechanical properties [10,11], such as dual-phase steel, which consists of an island of strong martensite second phase in a soft ferrite matrix. During plastic deformation, the plastic deformation of the soft zones is constrained by the elastic strain of the hard zones, generating back stress in the soft zones and forward stress in the hard zones. Back stress is a long-range internal stress generated by geometrically necessary dislocations (GNDs), sometimes in the form of dislocation pileups. Forward stress is generated in the hard zone to counterbalance the stress concentration at the zone boundary caused by back stress. This interactive force causes hetero-deformation-induced (HDI) strengthening (a kinematic stress), which increases the yield strength and enhances strain hardening, helping to maintain the ductility [9]. At the early stage of elastoplastic deformation before global yielding, the hard zones remain elastic and back stress plays a dominant role in enhancing the global yield strength in heterostructured materials [11]. The beneficial effects of the HDI strengthening have been reported to break the strength–toughness trade-off in pure metals [12], dual-phase alloys [13], austenitic stainless steels [14–16], high-entropy alloys [17], and so on.

The newly reported advanced strengthening and toughening mechanisms in steels are mainly for austenite containers, such as twinning or transformation-induced plasticity steel and dual-phase steel, based on the high work-hardening rate of FCC austenite [18–21]. In 4340 steels, austenite is stable at a high holding temperature, but nothing remains after quenching, due to a lack of sufficient austenite-stabilizing elements. Here, the intercritical quenching treatment [22] was employed to introduce bulk ferrite phase into tempered pearlite, creating a topography of heterogeneous microstructure, which is different from the conventional dual-phase steel. So far, the HDI strengthening effect in the above heterostructured steel has not been reported. This study focuses on this issue and investigates the relationship between quenching temperature and microstructure property. In addition, the contribution of the HDI strengthening and hardening effect to the improved mechanical properties was evaluated.

2. Materials and Methods

The chemical composition of experimental steel contains Fe-0.40C-0.22Si-0.65Mn-0.76Cr-1.35Ni-0.19Mo (wt.%). In order to achieve the above-mentioned objectives, the experimental steels are processed in three basic steps, including normalized annealing, quenching, and tempering; the schematic illustration is shown in Figure 1. First of all, the 4340 steel with a thickness of ~1 mm was normalized at 860 °C for 1 h followed by forced air cooling, to eliminate chemical composition inhomogeneity and residual stress. This is of great importance because the undissolved carbides from incomplete austenitization would have a great influence on the fracture properties of tempered samples [23]. After normalization, a mixed microstructure consisting of pearlite and a small amount of proeutectoid ferrite would be obtained. According to the measured dilatometric curves, the critical transformation temperature A_{c1} and A_{c3} were ~710 °C and 790 °C, respectively. To introduce different ferrite contents in the quenched microstructure, different quenching temperatures (720, 750, 780, 810, 840 °C) were set, and the holding time was 0.5 h followed

by water cooling. Finally, all quenched samples were tempered at 500 °C for 2 h followed by water cooling to room temperature.

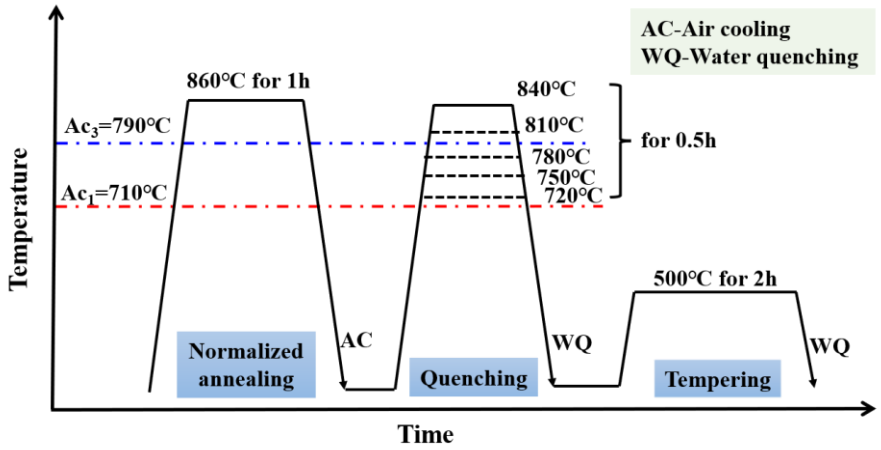

Figure 1. Schematic illustration of the applied heat treatment.

Microstructure observation of experimental steel was performed in a field emission scanning electron microscope (SEM, FEI Quanta 250F, USA) and a transmission electron microscope (TEM, FEI TECNAI 20, Brno, Czech Republic). The SEM samples were ground using successively finer SiC papers of #320, #600, #1000, and #1500. The ground specimens were then mechanically polished with 3.5 µm particle size diamond suspensions. After polishing, the samples were finally etched with 4% nitric acid alcohol solution for tens of seconds to reveal microstructural features. The SEM examinations were performed at an operating voltage of 15 kV and a working distance of ~10 mm. For TEM observation, the thin foils were first mechanically ground to a thickness of ~50 µm, then punched to prepare round disks of 3 mm in diameter, and finally, the disks were twin-jet (Tenupol-5) electro-polished in a solution of 80 mL perchloric acid and 920 mL ethanol at a potential of 30 V and −25 °C. The TEM specimens were examined at an acceleration voltage of 200 kV.

The Vickers hardness was measured in a micro-hardness tester (HMV-G21DT, Shimadzu Co., Tokyo, Japan) using a load of ~4.9 N with a dwell time of 15 s. Each hardness value shown is the average of 10 indentations. Quasi-static uniaxial tensile tests were performed in an Instron 5982 testing machine (Instron Company, Grove City, OH, USA) at a strain rate of 10^{-3} s^{-1} at room temperature. A self-developed contactless strain gauging system based on DIC (digital image correlation) technique (Nanjing, China) was applied to monitor the tensile strain during loading. Tensile specimens with a gauge length of 5 mm and a width of 2 mm were prepared by electrical discharge machining from the annealed sheets. Three tensile tests were repeated for each specimen to ensure the reproducibility of the data. The cyclic load–unload–reload (LUR) tests were carried out to measure the Bauschinger effect. During the LUR testing, the samples were tensioned to an assigned strain, then unloaded to 50 N at an unloading rate of 30 N/s, and then reloaded and unloaded again.

3. Results and Discussion

Typical SEM and TEM micrographs of the experimental steel after quenching at 720–840 °C are shown in Figures 2 and 3, respectively. After quenching at 720 °C, which is 10 °C above the A_{c1} temperature, a great amount of carbide precipitates were scattered inside the ferrite grains or at the ferrite grain boundaries, and a portion of fine isolated martensite (M) is also formed between the ferrite bulk, as shown in Figure 2a. These ferrite grains are irregular or equiaxed with a high density of dislocations near the phase boundaries between martensite and ferrite (Figure 3a). As the temperature is increased up to 750 °C, the samples mainly consist of quenched martensite accompanied by ~35% (in area fraction) undissolved ferrite (F_q) and a small number of carbides (Figure 2b). When

annealed at 780 °C for 0.5 h followed by water quenching, the fraction of ferrite further decreases to ~29% and only a few of carbides can be trapped (Figure 2c). A fully lath-type martensite structure can be achieved after quenching at temperatures higher than 810 °C (20 °C above the complete austenitization temperature A_{c3}), as shown in Figure 2d,e. The higher the quenching temperature, the larger the prior-austenite grains, and the wider the quenched martensitic laths. Obviously, the width of the martensitic lath decreases from 300 nm to 220 nm as the quenching temperature decreases from 840 °C to 780 °C (Figure 3b,c).

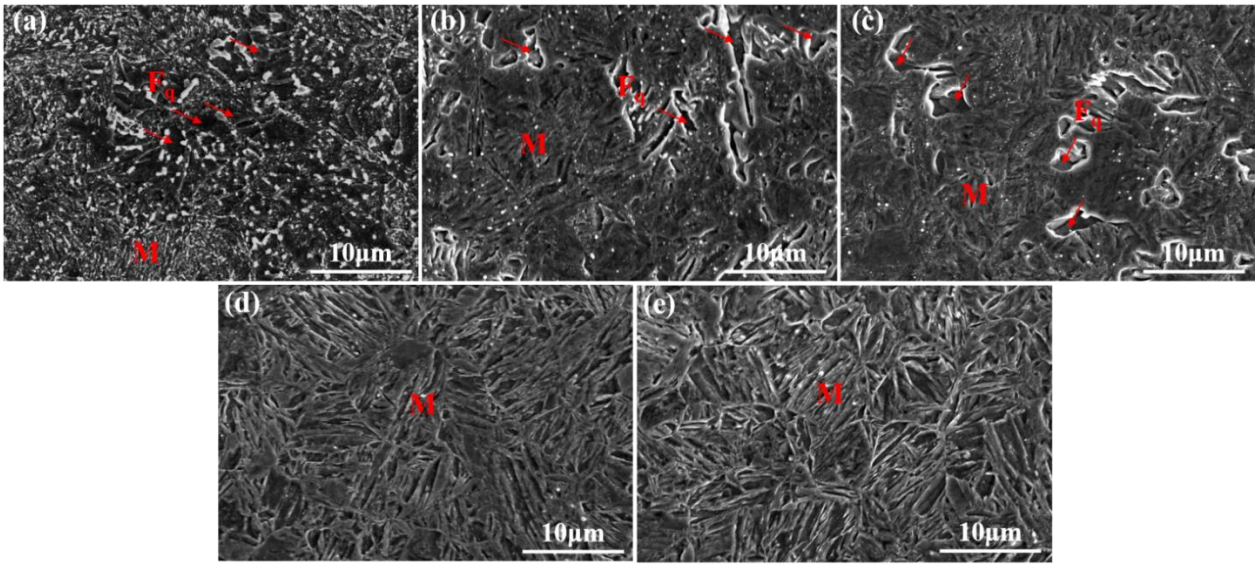

Figure 2. SEM images of experimental steel after quenching at (**a**) 720 °C, (**b**) 750 °C, (**c**) 780 °C, (**d**) 810 °C, and (**e**) 840 °C, respectively, showing microstructural evolution features. M and F_q refer to quenched martensite and undissolved ferrite, respectively.

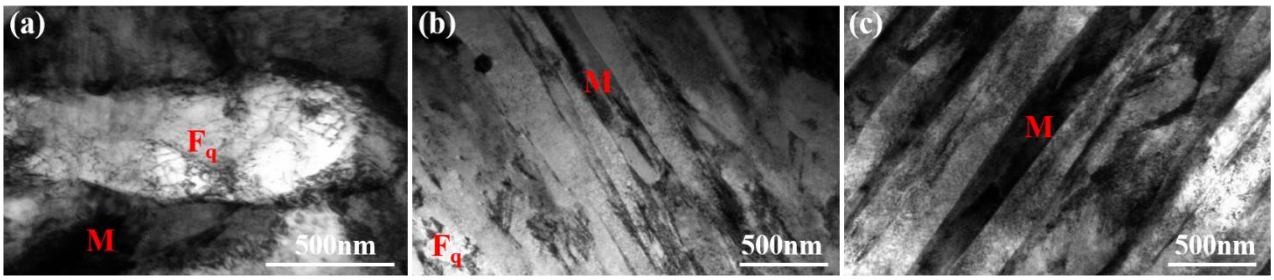

Figure 3. Typical TEM micrographs of samples after quenching at (**a**) 720 °C, (**b**) 780 °C, and (**c**) 840 °C.

The above results reveal that the shape, size, and volume fraction of the martensite/ferrite phases can be tuned by changing the quenching temperature. By this way, the prepared alloys will have the microstructure mixed with martensite and cementite (hard zones) and ferrite (soft zones). As is well known, the presence of terrible residual stresses in the quenched martensite has been associated with harmful impacts on the processing efficiency of the alloy, resulting in serious deformations; even cracking of the finished parts and components [24]. Subsequent tempering is considered to be helpful in releasing these terrible residual stresses. Through trial and error, holding for 2 h at 500 °C was selected to be an optimal tempering process.

In the process of tempering, the metastable martensite phase will decompose into ferrite and cementite, and the prior ferrite bulk (i.e., F_q) will be retained. For the sake of simplicity, the quenching temperature was used to label the samples to distinguish

one from the other, such as the 840–500 sample, which means the sample was quenched from 840 °C and then tempered at 500 °C for 2 h. Figure 4 demonstrates the effect of quenching temperature on the final tempered structure. Two types of ferrite structure can be observed in Figure 4a–c, respectively, obtained from the tempered samples quenched from 720–780 °C (intercritical quenching treatment). One is the micro-sized ferrite bulk (denoted as F_q) without carbides (Figure 4a–c); the other is the ultra-fine ferrite matrix containing dispersed cementite particles (pearlitic structure, marked by P). Statistics suggest that there is approximately 45% bulk ferrite in the area fraction in sample 720–500. The corresponding bright-field TEM image (Figure 5a) shows that the equiaxed ultrafine-grained ferrite grains contained a few of dislocations and precipitates; however, the ferrite matrix in the pearlitic structure has a significant diffraction contrast contributed to by abundant cementite or carbide particles and dislocations. In samples 750–500 and 780–500 (Figure 4b,c), the same heterostructures are also observed, but the area fraction of the prior ferrite bulk has been reduced to ~38% and 31%, respectively. A typical TEM micrograph in Figure 5b shows that in the 780–500 sample, cementite particles are located at the prior austenite grain boundaries (PAGBs), lath boundary, and the interior of the lath-type structures, which is in agreement with previous work [25]. While the sample was quenched at temperatures above the A_{c3} line, a representative pearlite structure is observed without any residual pure ferrite bulk, as shown in Figure 4d,e, and a large number of granular cementite precipitates filled the ferrite matrix. The enlarged TEM image (Figure 5c) reveals that a good deal of needle-like cementite particles embedded in ferrite grains, and numerous film-like cementite particles (the red arrow) located on the ferrite grain boundaries.

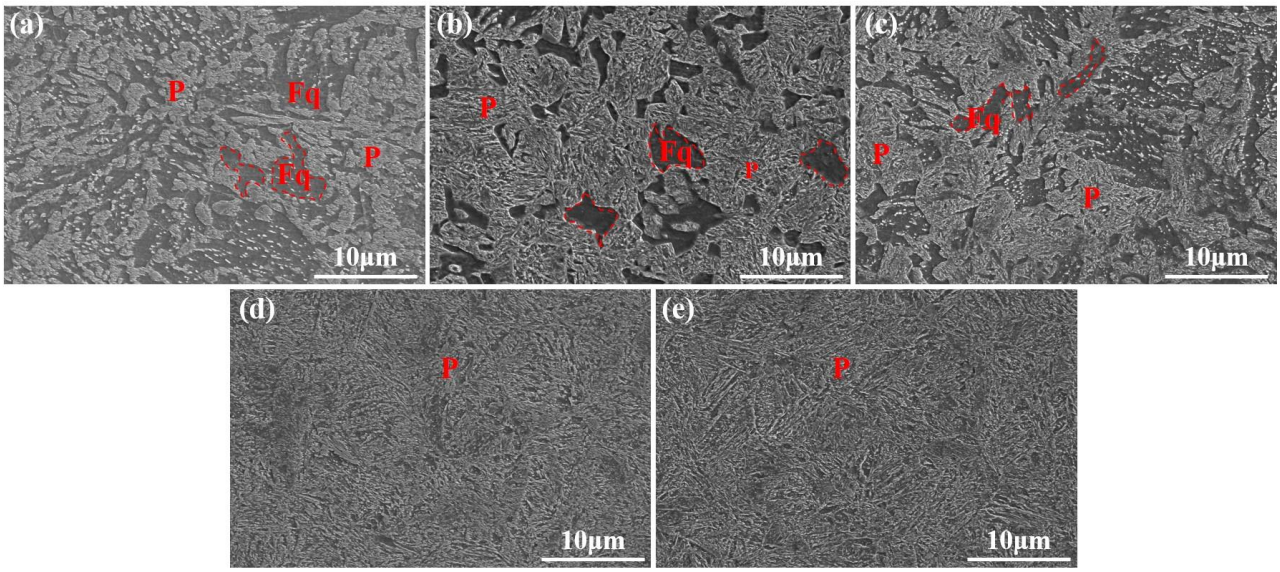

Figure 4. SEM images of the tempered steels after quenching from (**a**) 720 °C, (**b**) 750 °C, (**c**) 780 °C, (**d**) 810 °C, and (**e**) 840 °C, respectively. P and F_q refer to tempered pearlite structure and retained ferrite grains, respectively.

Based on the above, a novel heterostructure configuration and a classical pearlite structure can be achieved by controlling the quenching temperature. Besides the residual ferrite bulk, the pearlite zones in the heterostructure are different from the classical pearlite structure; the former has larger granular cementite particles, while the latter contains film- and needle-like cementite particles. Moreover, the density of carbide precipitates in the pearlite zones in the heterostructure is higher than that in the classical pearlite structure, because almost the same carbon content precipitates in the smaller volume.

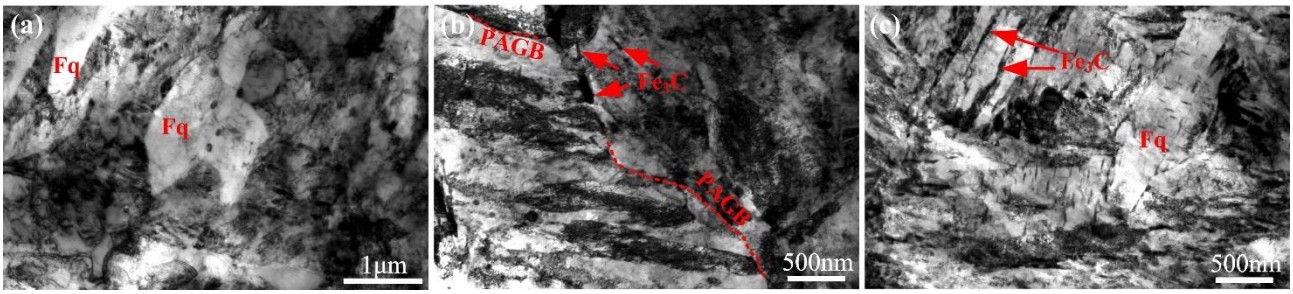

Figure 5. Typical bright-field TEM micrographs of tempered samples (**a**) 720–500 °C, (**b**) 780–500 °C, and (**c**) 840–500 °C.

Figure 6 gives the microhardness variation of the experimental steels as a function of the quenching temperature. As the quenching temperature increases from 720 °C to 840 °C, the microhardness of both the quenched and tempered samples first raises rapidly and then decreases slowly, and the highest hardness of both the quenched and tempered samples is obtained at 780 °C quenching temperature. The peak hardness of the quenched sample is about 760 HV, and that of the corresponding tempered sample is approximately 450 HV. For the quenched steels, the increase in hardness before 780 °C is mainly due to the lattice distortion caused by the formation of supersaturated martensitic structure. As is well documented, a higher martensite content would cause greater residual stresses and a higher dislocation density within the adjacent ferrite phase, resulting in a significant enhancement in strength as well as hardness of dual-phase steels [26,27]. As the quenching temperature was further increased to complete austenization areas (above 810 °C), slight softening occurred. This should be ascribed to the reduction of average C content in the lath-type martensite structure and the widening of martensite lath, as shown in Figure 3. While for the tempered specimens, the formation of more pearlite zones should be responsible for the hardness variation with increasing quenching temperature before 780 °C, and the hardness drop results from the decrease in the density of cementite particles in the ferrite matrix with the gradual disappearance of the residual ferrite bulk, referring to Figures 3 and 4.

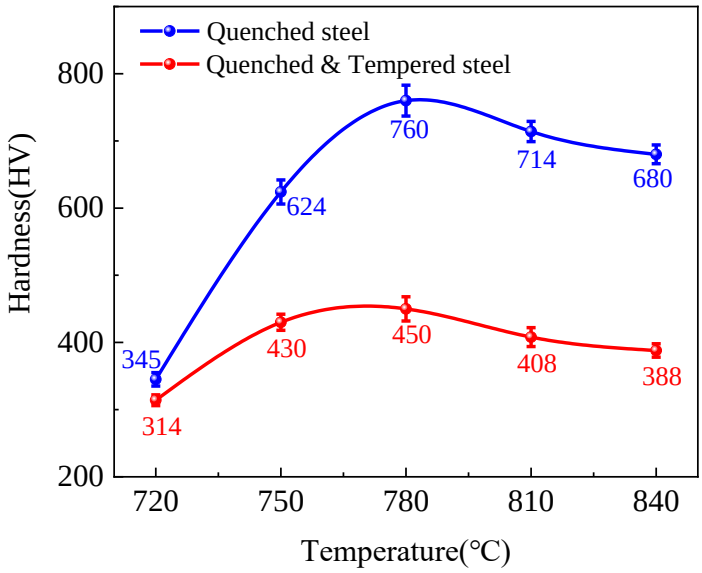

Figure 6. Variation of microhardness of quenched and tempered steels as a function of quenching temperature.

The engineering stress-engineering strain plots of the tempered samples exhibit continuous yielding, as shown in Figure 7a. The effect of the quenching temperature on the tensile properties is summarized in Figure 7b and Table 1. The variation of the strength is

similar to that of the hardness, undergoing the undulation of rising first and then falling. In view of the microstructure, the strength of the steel varies with the decrease in the residual ferrite zones; that is, the strength increases with the decrease in the residual ferrite zones at the first stage, and then reaches the peak with 31% residual ferrite zones in the area fraction, and finally slowly decreases as the ferrite zones gradually disappear. The highest tensile strength and yield strength are 1300 MPa and 1230 MPa, respectively, both at 780 °C quenching temperature. However, the tensile strength and yield strength of the pearlite steel quenched from 840 °C are 1233 MPa and 1156 MPa, respectively, and are reduced by 67 MPa and 74 MPa compared with the peak strength. When the quenching temperature goes down a little to 810 °C, still above the A_{c3} line, it has little impact on the strength of steel with pearlite structure. However, as the temperature drops from the A_{c3} line to the A_{c1} line, the strength of the steel dwindles fast, along with the volume shrinkage of the residual ferrite zones in the microstructure. The most noteworthy feature of the strength change is that the peak is achieved in the sample where there is about 31 vol.% residual ferrite bulk (Figure 3c), which is contrary to traditional knowledge.

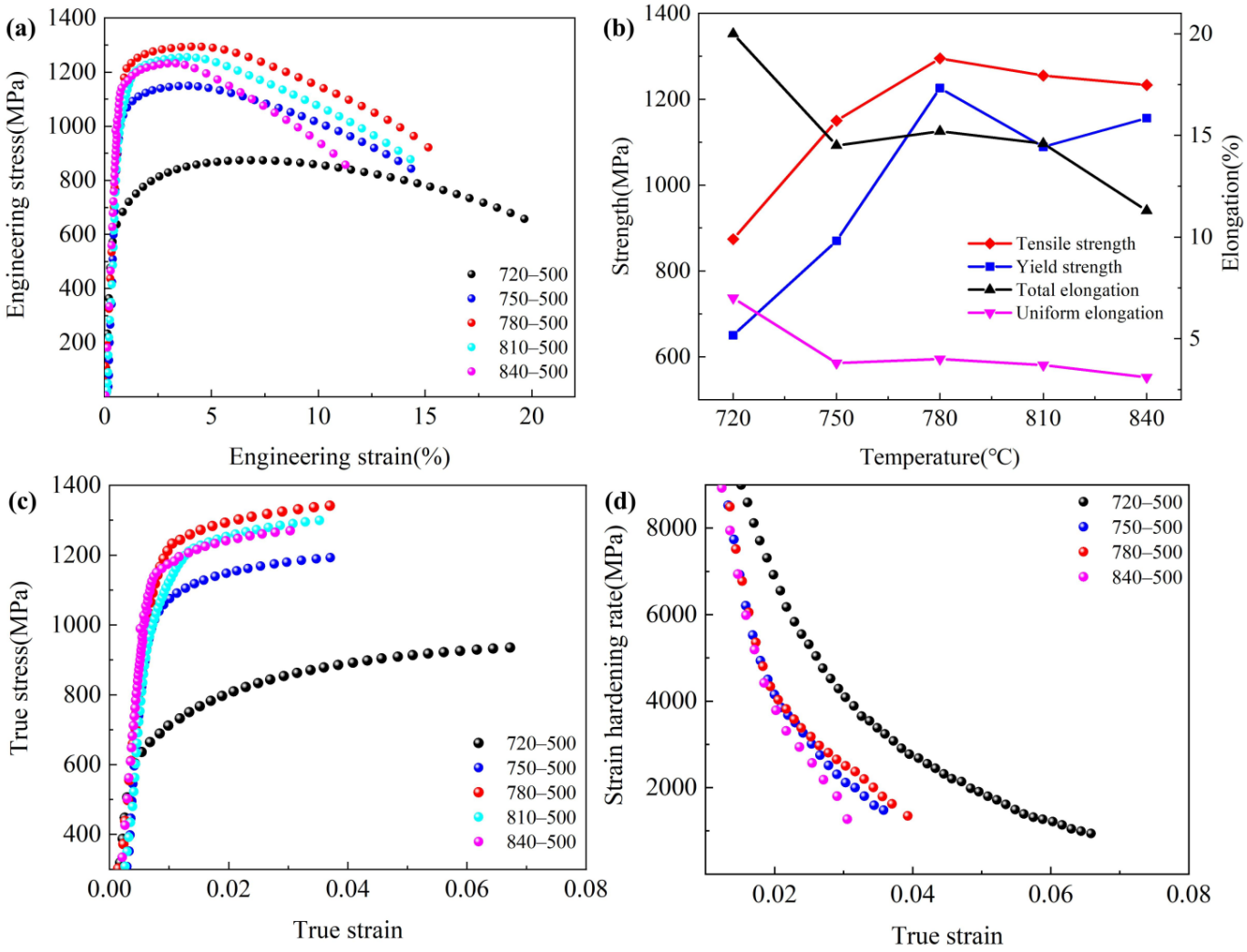

Figure 7. Effects of quenching temperature on mechanical properties of experimental steels. (**a**) engineering stress-engineering strain curves, (**b**) strength and elongation of tempered steels as a function of quenching temperature, (**c**) true stress-true strain plots, and (**d**) work hardening rate-true strain curves of tempered samples.

Table 1. Mechanical properties of quenched and tempered steels.

Sample	Tensile Strength, MPa	Yield Strength, Mpa	Uniform Elongation, %	Total Elongation, %
720–500	874	650	7	20
750–500	1150	870	3.8	14.5
780–500	1295	1226	4	15.2
810–500	1255	1089	3.7	14.6
840–500	1233	1156	3.1	11.3

As is well known, the strength and ductility (uniform elongation) of materials move in perfect opposition when the materials are strengthened by traditional methods. Excitingly, the results shown in Figure 7a,b exhibit a breakthrough against the traditional knowledge, and the uniform elongation remains more or less constant at 4%, except for the sample 720–500, although the strength changes. The calculated true stress-strain plots and corresponding work hardening rate curves are shown in Figure 7c,d, respectively. All strain hardening rate curves include a rapid drop before 0.02 and a slow decline after 0.02. The section after 0.02 reveals the work hardening ability of the sample in the process of plastic deformation. Obviously, the more residual ferrite bulk there is, the higher the working hardening rate. The introduction of residual ferrite bulk benefits the alloy in gaining good strain-hardening capability. Thus, the 720–500 steel possessed the highest work hardening ability due to the larger fraction of ferrite (the black line in Figure 7d). The strain energy density, another parameter of toughness, was calculated to be 159.6 MJ/m^3 in 720–500 vs. 147.8 MJ/m^3 in 750–500 vs. 174 MJ/m^3 in 780–500 vs. 158.7 MJ/m^3 in 810–500 vs. 121.5 MJ/m^3 in 840–500, according to the area below the engineering stress-engineering strain curve. Both the enhancement strain-hardening capability and strain energy density indicate a notable gain in toughness in the 780–500 sample with optimized heterostructure, compared to that of the 840–500 sample with classical pearlite structure.

Combined, the heterostructured steel has excellent comprehensive mechanical properties with a higher tensile strength of 1300 MPa, an enhanced yield strength of 1230 MPa, and better toughness, indicated by the enhancement strain-hardening capability and strain energy density. The superior mechanical property is related to the content of residual bulk ferrite, which optimizes carbon partition and provides dislocation motion. Generally, ferrite is almost carbon-free, hence the average carbon content in the quenched martensite in 780–500 steels is relatively higher than that in samples annealed at a complete austenitizing temperature, leading to a higher density of carbides in the corresponding tempered structure. Therefore, the loss of strength and hardness caused by the formation of the ferrite phase can be compensated by that caused by the enhanced precipitation strengthening. In addition, strain partitioning and a strain gradient can be generated during the tensile deformation near the boundaries between the soft ferrite zones and hard pearlite ones, to ensure the continuity of deformation. Thus, the GNDs would be created near the soft/hard zone boundaries, producing a long-range stress (back stress), which would provide extra strain hardening [11].

As to validate the above assumption, the contribution of HDI hardening to the overall strength of experimental steels is evaluated according to the measured LUR hysteresis loops (Figure 8a) and the following equations [28].

$$\sigma_{HDI} = \sigma_{flow} - \sigma_{eff} \quad (1)$$

$$\sigma_{eff} = \frac{\sigma_{flow} - \sigma_u}{2} + \frac{\sigma^*}{2} \quad (2)$$

where σ_{flow}, σ_{eff} and σ_u are flow stress, effective stress, and reverse yield stress, respectively, and σ^* represents the thermal component of the flow stress related to viscous flow at the initiation of unloading, as schematically defined in Figure 8b.

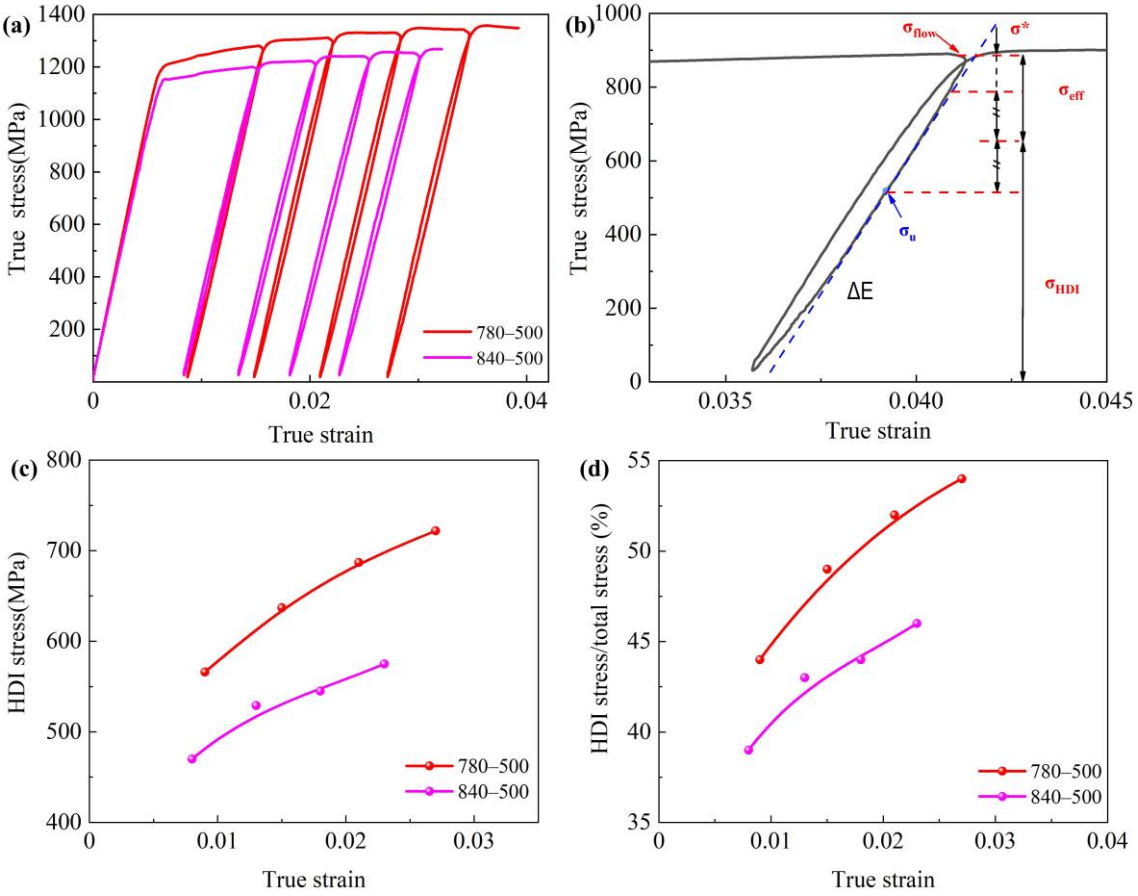

Figure 8. Bauschinger effect and HDI stress of the tempered steels. (**a**) LUR stress-strain curves, (**b**) schematic of hysteresis loops for calculating HDI stress, (**c**) HDI stress versus applied strain, (**d**) contribution of HDI stress to total stress as a function of true strain.

The calculated HDI stress values as a function of the true strain are summarized in Figure 8c, and it can be seen that the HDI stress grows almost linearly with the applied true stress for the selected samples. Predictably, the tempered sample quenched from 780 °C has higher HDI stress in the range of 560 MPa to 720 MPa throughout the whole deformation process, compared to the 840–500 samples (470~575 MPa). Figure 8d lists the contribution of HDI stress to the total stress throughout the deformation, and also the contribution of HDI stress to the total stress is much higher in the tempered sample quenched from 780 °C. As mentioned above, about a 31% fraction of ferrite was introduced in the 780–500 steel, and the soft phase (F_q) was constrained by a tempered pearlite structure (P) (regarded as the hard zones). This provided direct experimental evidence for the effects of heterostructure on mechanical properties, which is consistent with the report that the highest HDI hardening is achieved when the content of soft zones was around ~30 vol.% in heterostructured materials [11]. The extra strain hardening provided by HDI stress is responsible for the good combination of strength and ductility achieved in the tempered sample after quenching from 780 °C.

4. Conclusions

Based on the concept of heterogeneous structure, intercritical quenching plus tempering treatments were used to modify the microstructural characteristics of a 4340 steel. The effect of quenching temperature on the microstructure evolution and mechanical property was investigated, and the microstructure–property relationship was established. In addition, the contribution of HDI stress to the improvement of strength and ductility was evaluated. Some interesting conclusions can be drawn as follows:

(1) As the quenching temperature increased from 720 °C to 840 °C, the area fraction of undissolved ferrite in the quenched samples decreased, and the cementite also gradually decomposed completely. For the corresponding tempered steels, the microstructural constituents changed from 45% residual ferrite and tempered pearlite in the 720–500 sample, to 31% ferrite plus pearlite structure in the 780–500 steel, and finally to complete pearlite in the 840–500 one.
(2) The heterostructured steel (HS, i.e., 780–500 sample) exhibits superior mechanical properties compared to the pearlite steel (PS, i.e., 840–500 sample): 1300 MPa in HS vs. 1233 MPa in PS for tensile strength, 1230 MPa in HS vs. 1156 MPa in PS for yield strength, 174 MJ/m^3 in HS vs. 121.5 MJ/m^3 in PS for strain energy density (toughness), and better strain-hardening capability.
(3) The volume fraction of the soft ferrite bulk zone has a decisive influence on the HDI strengthening. Here, the heterostructured steel exhibits the best HDI hardening ability when it has 31% residual ferrite zones in the volume fraction, which can be achieved by quenching at 780 °C following the tempering at 500 °C for 2 h.

Author Contributions: Conceptualization, J.L.; methodology and investigation, Y.S. and G.S.; data collection and analysis, Y.S. and G.S.; writing—review & editing, Y.S., G.S. and J.L. All authors have read and agreed to the published version of the manuscript.

Funding: This work was supported by the Natural Science Foundation of Jiangsu Province (grant numbers BK20201308 and BK20220964). The authors are thankful for the technical support from the Jiangsu Key Laboratory of Advanced Micro & Nano Materials and Technology, the Analysis and Test Center of Nanjing University of Science and Technology.

Data Availability Statement: The data presented in this study are available on request from the corresponding author.

Conflicts of Interest: The authors declare no conflict of interest.

References

1. Saeidi, N.; Ekrami, A. Comparison of mechanical properties of martensite/ferrite and bainite/ferrite dual phase 4340 steels. *Mater. Sci. Eng. A* **2009**, *523*, 125–129. [CrossRef]
2. Moraes, D.A.; Almeida, G.F.C.; Couto, A.A.; Massi, M.; Caliari, F.R.; Lima, C.R.C. Creep of High-Strength Steel Coated with Plasma Sprayed Self-Fluxing Alloy. *Metals* **2023**, *13*, 763. [CrossRef]
3. Lopez-Garcia, R.D.; Medina-Juárez, I.; Maldonado-Reyes, A. Effect of Quenching Parameters on Distortion Phenomena in AISI 4340 Steel. *Metals* **2022**, *12*, 759. [CrossRef]
4. Goanță, V.; Munteanu, C.; Müftü, S.; Istrate, B.; Schwartz, P.; Boese, S.; Ferguson, G.; Morăraș, C.-I.; Stefan, A. Evaluation of the Fatigue Behavior and Failure Mechanisms of 4340 Steel Coated with WIP-C1 (Ni/CrC) by Cold Spray. *Materials* **2022**, *15*, 8116. [CrossRef] [PubMed]
5. Clarke, A.J.; Miller, M.K.; Field, R.D.; Coughlin, D.R.; Gibbs, P.J.; Clarke, K.D.; Alexander, D.J.; Powers, K.A.; Papin, P.A.; Krauss, G. Atomic and nanoscale chemical and structural changes in quenched and tempered 4340 steel. *Acta Mater.* **2014**, *77*, 17–27. [CrossRef]
6. Lee, W.S.; Su, T.T. Mechanical properties and microstructural features of AISI 4340 high-strength alloy steel under quenched and tempered conditions. *J. Mater. Process. Technol.* **1999**, *87*, 198–206. [CrossRef]
7. Wu, X.L.; Zhu, Y.T. Heterogeneous materials: A new class of materials with unprecedented mechanical properties. *Mater. Res. Lett.* **2017**, *5*, 527–532. [CrossRef]
8. Miura, H.; Kobayashi, M.; Todaka, Y.; Watanabe, C.; Aoyagi, Y.; Sugiura, N.; Yoshinaga, N. Heterogeneous nanostructure developed in heavily cold-rolled stainless steels and the specific mechanical properties. *Scr. Mater.* **2017**, *133*, 33–36. [CrossRef]
9. Zhu, Y.T.; Wu, X.L. Perspective on hetero-deformation induced (HDI) hardening and back stress. *Mater. Res. Lett.* **2019**, *9*, 393–398. [CrossRef]
10. Estrin, Y.; Beygelzimer, Y.; Kulagin, R.; Gumbsch, P.; Fratzl, P.; Zhu, Y. Architecturing materials at mesoscale: Some current trends. *Mater. Res. Lett.* **2021**, *9*, 399–421. [CrossRef]
11. Zhu, Y.T.; Ameyama, K.; Anderson, P.M.; Beyerlein, I.J.; Gao, H.; Kim, H.S.; Lavernia, E.; Mathaudhu, S.; Mughrabi, H.; Ritchie, R.O.; et al. Heterostructured materials: Superior properties from hetero-zone interaction. *Mater. Res. Lett.* **2021**, *9*, 1–31. [CrossRef]
12. Wu, X.L.; Yang, M.X.; Yuan, F.P.; Wu, G.; Wei, Y.; Huang, X.; Zhu, Y. Heterogeneous lamella structure unites ultrafine-grain strength with coarse-grain ductility. *Proc. Natl. Acad. Sci. USA* **2015**, *112*, 14501–14505. [CrossRef] [PubMed]

13. Huang, J.X.; Liu, Y.; Xu, T.; Chen, X.F.; Lai, Q.Q.; Xiao, L.R.; Pan, Z.Y.; Gao, B.; Zhou, H.; Zhu, Y.T. Dual-phase hetero-structured strategy to improve ductility of a low carbon martensitic steel. *Mater. Sci. Eng. A* **2022**, *834*, 142584. [CrossRef]
14. Wu, X.L.; Yang, M.X.; Yuan, F.P.; Chen, L.; Zhu, Y. Combining gradient structure and TRIP effect to produce austenite stainless steel with high strength and ductility. *Acta Mater.* **2016**, *112*, 337–346. [CrossRef]
15. Sun, G.S.; Liu, J.Z.; Zhu, Y.T. Heterostructure alleviates Lüders deformation of ultrafine-grained stainless steels. *Mater. Sci. Eng. A* **2022**, *848*, 143393. [CrossRef]
16. Hu, J.; Li, X.Y.; Zhang, Z.M.; Wang, L.; Li, Y.; Xu, W. Overcoming the strength-ductility trade-off in metastable dual-phase heterogeneous structures using variable temperature rolling and annealing. *Mater. Res. Lett.* **2023**, *11*, 648–654. [CrossRef]
17. Li, Z.; Pradeep, K.G.; Deng, Y.; Raabe, D.; Tasan, C.C. Metastable high-entropy dual-phase alloys overcome the strength–ductility trade-off. *Nature* **2016**, *534*, 227–230. [CrossRef]
18. Hu, J.; Zhang, J.M.; Sun, G.S.; Du, L.X.; Liu, Y.; Dong, Y.; Misra, R.D.K. High strength and ductility combination in nano-/ultrafine-grained medium-Mn steel by tuning the stability of reverted austenite involving intercritical annealing. *J. Mater. Sci.* **2019**, *54*, 6565–6578. [CrossRef]
19. Jing, S.; Ding, H.; Ren, Y.; Cai, Z. A new insight into annealing parameters in tailoring the mechanical properties of a medium Mn steel. *Scr. Mater.* **2021**, *202*, 114019. [CrossRef]
20. He, B.B.; Hu, B.; Yen, H.W.; Cheng, G.J.; Wang, Z.K.; Luo, H.W.; Huang, M.X. High dislocation density–induced large ductility in deformed and partitioned steels. *Science* **2017**, *357*, 1029–1032. [CrossRef]
21. Luo, Z.C.; Huang, M.X. Revisit the role of deformation twins on the work-hardening behaviour of twinning-induced plasticity steels. *Scr. Mater.* **2018**, *142*, 28–31. [CrossRef]
22. Mehrabi, A.; Sharifi, H.; Asadabad, M.A.; Reza, A.N.; Ali, R. Improvement of AISI 4340 steel properties by intermediate quenching–microstructure, mechanical properties, and fractography. *Int. J. Mater. Res.* **2020**, *111*, 711–779. [CrossRef]
23. Clarke, A.J.; Klemm-Toole, J.; Clarke, K.D.; Coughlin, D.R.; Pierce, D.T.; Euser, V.K.; Poplawsky, J.D.; Clausen, B.; Brown, D.; Almer, J.; et al. Perspectives on quenching and tempering 4340 steel. *Metall. Mater. Trans. A* **2020**, *51*, 4984–5005. [CrossRef]
24. Samuel, A.; Prabhu, K.N. Residual stress and distortion during quench hardening of steels: A review. *J. Mater. Eng. Perform.* **2022**, *31*, 5161–5188. [CrossRef]
25. Lim, N.S.; Bang, C.W.; Das, S.; Jin, H.W.; Ayer, R.; Park, C.G. Influence of tempering temperature on both the microstructural evolution and elemental distribution in AISI 4340 steels. *Met. Mater. Int.* **2012**, *18*, 87–92. [CrossRef]
26. Hosseinifar, F.; Ekrami, A. The effect of cold-rolling prior to the inter-critical heat treatment on microstructure and mechanical properties of 4340 steel with ferrite–martensite microstructure. *Mater. Sci. Eng. A* **2022**, *830*, 142314. [CrossRef]
27. Gao, B.; Hu, R.; Pan, Z.Y.; Chen, X.; Liu, Y.; Xiao, L.; Cao, Y.; Li, Y.; Lai, Q.; Zhou, H. Strengthening and ductilization of laminate dual-phase steels with high martensite content. *J. Mater. Sci. Technol.* **2021**, *65*, 29–37. [CrossRef]
28. Yang, M.X.; Pan, Y.; Yuan, F.P.; Zhu, Y.; Wu, X. Back stress strengthening and strain hardening in gradient structure. *Mater. Res. Lett.* **2016**, *4*, 145–151. [CrossRef]